

LETTER • OPEN ACCESS

Intense XUV pulses from a compact HHG setup using a single harmonic

To cite this article: M Kretschmar *et al* 2021 *J. Phys. B: At. Mol. Opt. Phys.* **54** 20LT01

View the [article online](#) for updates and enhancements.

You may also like

- [Impact of Catalyst Performance on the Life-Cycle CO₂ Emissions of Methanol Production By Direct Electrocatalytic Reduction of CO₂](#)
Matthew Pellow and Sally Benson
- [Research on the Influence of Shear Turbulence on the Aerodynamic Loads Characteristics of Wind Turbine](#)
Tong Tong, Bangxing Li and Xin Ren
- [The relationship of the morphological characteristics of some varieties of soybean on the attack intensity of the pod borer \(*Etiella zinckenella* Treitschke\) in two different cultivation techniques](#)
B A Patu, M Sarjan, Tarmizi *et al.*



IOP | ebooks™

Bringing together innovative digital publishing with leading authors from the global scientific community.

Start exploring the collection—download the first chapter of every title for free.

Letter

Intense XUV pulses from a compact HHG setup using a single harmonic

M Kretschmar, M J J Vrakking  and B Schütte* 

Max-Born-Institut, Max-Born-Straße 2A, 12489 Berlin, Germany

E-mail: Bernd.Schuette@mbi-berlin.de

Received 29 June 2021, revised 6 October 2021

Accepted for publication 5 November 2021

Published 29 November 2021

**Abstract**

We report on a compact and spectrally intense extreme-ultraviolet (XUV) source, which is based on high-harmonic generation (HHG) driven by 395 nm pulses. In order to minimize the XUV virtual source size and to maximize the XUV flux, HHG is performed several Rayleigh lengths away from the driving laser focal plane in a high-density gas jet. As a result, a high focused XUV intensity of $5 \times 10^{13} \text{ W cm}^{-2}$ is achieved, using a beamline with a length of only two meters and a modest driving laser pulse energy of 3 mJ. The high XUV intensity is demonstrated by performing a nonlinear ionization experiment in argon, using an XUV spectrum that is dominated by a single harmonic at 22 eV. Ion charge states up to Ar^{3+} are observed, which requires the absorption of at least four XUV photons. The high XUV intensity and the narrow bandwidth are ideally suited for a variety of applications including photoelectron spectroscopy, the coherent control of resonant transitions and the imaging of nanoscale structures.

Keywords: XUV, nonlinear optics, extreme-ultraviolet, attosecond, coherent diffractive imaging, strong-field physics, photoelectron spectroscopy


(Some figures may appear in colour only in the online journal)

Ultrashort, intense extreme-ultraviolet (XUV) pulses are used in a growing number of applications, which include nonlinear multiphoton ionization of atoms [1–6], molecules [7, 8] and clusters [9–11], second-harmonic generation (SHG) in thin films [12] and the study of XUV strong-field physics [13, 14]. Intense XUV pulses are also a prerequisite for performing XUV-pump XUV-probe experiments where XUV pulse durations down to the attosecond regime have already been used [15–17]. While the study of electron dynamics on these extremely short time scales requires broadband XUV

pulses, intense XUV pulses with a narrower bandwidth are advantageous for a range of applications including photoelectron spectroscopy [18, 19] and the study of resonant transitions, e.g. within four-wave mixing [20], superfluorescence [21] and the control of Rabi oscillations [22]. Furthermore, XUV pulses with a narrow bandwidth and a high spectral intensity are ideally suited for single-shot coherent diffractive imaging (CDI) of nanostructures and nanoscale targets [23–25].

Narrowband intense XUV pulses are available from free-electron laser (FEL) facilities [26–28], but the limited access and the large size of these facilities can make experiments very challenging. Alternatively, long high-harmonic generation (HHG) beamlines with lengths around 10 meters or even longer have been developed for the generation of intense XUV pulses [4–6, 11, 15, 16, 29, 30]. Intense XUV sources based on

* Author to whom any correspondence should be addressed.

 Original content from this work may be used under the terms of the [Creative Commons Attribution 4.0 licence](https://creativecommons.org/licenses/by/4.0/). Any further distribution of this work must maintain attribution to the author(s) and the title of the work, journal citation and DOI.

HHG are currently being developed, including the user facilities ELI beamlines in Prague [31] and ELI-ALPS in Szeged [32]. A disadvantage of these sources is that they require very powerful laser systems for driving the HHG process, often reaching the multi-terawatt range. At the same time, these large-scale setups lead to high demands regarding the laser stability. This can be challenging, especially when considering that the XUV pulses are typically focused to micrometer or even nanometer spot sizes [33, 34] and that some of these experiments require attosecond stability. A number of more compact XUV sources have been reported that were used to study two-photon ionization and absorption in He, resulting in the generation of singly-charged He ions [35–37].

In state-of-the-art setups devoted to the generation of intense XUV pulses based on HHG, the focus often lies on maximizing the XUV flux by using powerful driving lasers and by loosely focusing the driving laser pulses into the HHG medium [4, 5, 32, 38]. Recently, we have used a different approach, demonstrating that optimization of the XUV intensity on target requires a choice of parameters entirely different from the parameters needed to optimize the XUV pulse energy [6]. This approach was based on using a modest focal distance (5 m) for the near-infrared (NIR) driving laser, followed by a long propagation distance of the generated XUV beam. This enables large demagnification of the XUV source size and resulted in a high XUV intensity of $7 \times 10^{14} \text{ W cm}^{-2}$. Using these pulses for multiphoton ionization, charge states up to Ar^{5+} were observed following the absorption of at least 10 XUV photons. At the same time, a moderate NIR pulse energy of 11 mJ was used [6]. However, this setup still required a lot of space, since overall an 18 m-long beamline was used.

An important consideration for the generation of intense XUV pulses is that optical elements should only be used where absolutely necessary, because these typically suffer from high reflection/transmission losses and/or aberrations. Furthermore, only modest demagnification of the XUV source size can be achieved even in complex optical arrangements, e.g. when three toroidal mirrors are used [39]. Instead, a promising path is to exploit the inherent properties of the generated XUV pulses. Recently, we demonstrated that generating high harmonics several Rayleigh lengths away from the driving laser focus can result in the generation of a large HHG volume and a small virtual XUV source size of only a few micrometers. After refocusing the XUV pulses, a high XUV intensity of $2 \times 10^{14} \text{ W cm}^{-2}$ was achieved in a compact setup with a length of only 2 meters [40], enabling triple ionization of argon atoms. In these experiments the XUV pulses used for the ionization of argon atoms consisted of four different harmonic orders, which made it difficult to understand the ionization pathways in detail.

Here we demonstrate the generation of intense narrowband XUV pulses in a simple and compact setup, where high harmonics are generated several Rayleigh lengths away from the driving laser focus in a short, high-density gas jet. The HHG is driven by the second harmonic of the fundamental NIR pulses, resulting in a large spectral separation between the individual harmonic orders. Using an Al filter to block the driving laser

and a normal-incidence XUV focusing mirror, an XUV pulse dominated by a single harmonic order at 22 eV is obtained. In the ionization of Ar atoms, Ar^{2+} and Ar^{3+} ions are observed, which requires the absorption of at least two and four XUV photons, respectively.

The concept for generating intense XUV pulses in a compact setup is presented in figure 1. First, NIR pulses centered at 790 nm with an energy of 13 mJ and a duration of 40 fs [41] at a repetition rate of 10 Hz were frequency-doubled in a 150 μm -thick beta-barium borate crystal by SHG, resulting in a pulse energy of 3 mJ at 395 nm. The bandwidth was 5.5 nm, corresponding to a transform-limited pulse duration of 42 fs. Assuming some chirp, a pulse duration of 50 fs was estimated. Two dichroic mirrors were used to separate the generated violet beam from the fundamental beam. Next, as shown in figure 1, these pulses were focused using a spherical lens with a focal length of 1 m, resulting in an estimated peak intensity of $8 \times 10^{15} \text{ W cm}^{-2}$ in the focal plane when no gas was present. High harmonics were generated in a high-density gas jet produced by a cantilever piezoelectric valve with a nozzle diameter of 0.5 mm [42] that was placed either before or behind the focal plane of the violet laser. By generating high harmonics several Rayleigh lengths away from the focal plane of the violet laser, curved wavefronts are transferred from the driving laser to the generated XUV beam (see lower graph in figure 1). As a consequence, the violet and the XUV beams are expected to have similar divergences. Due to the shorter wavelength, however, the XUV virtual source size is significantly smaller than the focus size of the driving laser (see also reference [40]). By further demagnifying the virtual XUV source size using a spherical mirror (coated with B_4C) with a short focal length of 75 mm, a high XUV intensity can be achieved using a setup that has a length of only 2 meters. An important advantage of generating harmonics in this scheme is the large generation volume leading to a comparably high XUV photon flux.

A 100 nm-thick Al filter was used to block the driving laser, while transmitting XUV photons with energies higher than about 16 eV. The XUV beam profile was recorded using a microchannel plate/phosphor screen assembly that was placed at a distance of about 50 cm from the gas jet. For the non-linear ionization of argon, a pulsed atomic jet of argon atoms was generated by a second cantilever piezoelectric valve with a nozzle diameter of 0.5 mm. The central part of the atomic jet was selected by a skimmer with an orifice diameter of 0.5 mm. Following interaction of the focused XUV beam with the atomic beam, the generated ions were recorded using a velocity-map imaging spectrometer (VMIS) [43] that was operated in spatial-map imaging mode [44]. Individual ion traces were separately recorded by gating the detector and changing the delay of the gating window.

Figure 2(a) shows the dependence of the obtained HHG yield in Kr using a backing pressure of 4 bar on the distance between the focal plane of the driving laser and the gas jet. This curve has a maximum at -1.5 cm , which means that the focus is located approximately 5 Rayleigh lengths before the gas jet. Under these conditions, both the XUV beam size at the jet and its divergence are expected to be similar to the size and

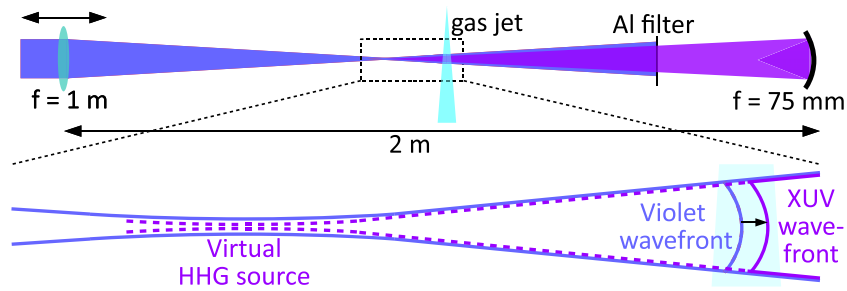


Figure 1. Compact intense XUV setup. A violet laser pulse at 395 nm is focused by a lens with a focal length of 1 m. High harmonics are generated in a gas jet that is placed several Rayleigh lengths away from the focal plane of the violet laser. As a result, both the size and the divergence of the generated XUV beam are similar to the size and the divergence of the driving laser. However, as shown in the zoomed region in the lower part of the graph, the virtual XUV source size is significantly smaller than the focal size of the violet laser, as a consequence of the shorter wavelength of the XUV beam. An Al filter is used to attenuate the violet laser beam. High XUV intensities are obtained by demagnifying the XUV source size using an XUV focusing element with a short focal length f . To this end, a spherical B₄C-coated mirror with $f = 75$ mm is used.

the divergence of the driving laser (see figure 1 and reference [40]). To obtain information about the width of the gas jet, the dependence of the HHG yield on the transverse position of the gas jet with respect to the driving laser beam was recorded, as presented in figure 2(b). This curve has a full width at half maximum (FWHM) of about 1 mm. Figure 2(c) depicts the relative HHG yield as a function of the backing pressure, which exhibits a steep increase up to about 1 bar. Saturation starts to set in at higher pressures, and from about 4 bar the HHG yield is almost constant. This is comparable to our previous results using 800 nm driving pulses, where this behavior was attributed to reshaping of the fundamental laser and its influence on phase-matching under these conditions [40]. The saturation behavior is advantageous, since it makes the HHG optimization comparably simple and because slightly different pressures experienced by the driving laser across its beam profile have a negligible effect on the spatially dependent HHG yield. From figure 2(c) one can extract that the HHG yield at 2 bar is about 77% of the HHG yield at 4 bar. Using this information in combination with the results shown in figure 2(b), we estimate that the region of the gas jet where the yield drops to 77% on both sides of the maximum (meaning that the pressure has dropped by a factor of about 2) spans a width of about 0.75 mm. This represents an estimation of the gas jet width and is in accordance with expectations, considering that the nozzle diameter of the gas valve is 0.5 mm and that the exit of the nozzle is placed as close to the laser beam as possible.

The XUV beam profile recorded at a distance of 50 cm behind the driving laser focus is presented as an inset in figure 3(a). The beam radius at this position is about 3 mm, corresponding to an FWHM divergence of 7 mrad, which is similar to the divergence of the violet laser and is a direct consequence of performing the HHG process several Rayleigh lengths away from the focal plane of the driving laser. In figure 3(a), a photoelectron spectrum is shown that was obtained after focusing the XUV beam into an Ar gas jet and by applying negative voltages to the electrodes of the VMIS. The spectrum is dominated by the contribution from a single harmonic order with a photon energy of about 22 eV, corresponding to the H7 of the violet driving laser (i.e. the

14th harmonic of the NIR laser). We note that spin-orbit coupling results in two electron peaks separated by 0.18 eV [45], which are, however, not resolved in this experiment. For comparison, figure 3(b) depicts a photoelectron spectrum obtained for the ionization of Kr, showing that the contributions from both the 5th and the 9th harmonics are small. Slightly different HHG conditions might be responsible for the fact that a contribution from the 9th harmonic is observed in figure 3(b), but not in figure 3(a). Generating harmonics using 395 nm driving pulses results in a small cutoff energy, which here lies between the 7th and 9th harmonics. We note that the intensity of the driving laser may be reduced in the gas jet by reshaping effects [40], which in turn reduces the HHG cutoff energy when compared to the driving laser intensity that would be obtained in vacuum. The dominance of a single harmonic was further facilitated by the large spectral separation between the harmonic orders (≈ 6.3 eV) and by exploiting the filtering characteristics of the Al filter (which has a high transmission for photon energies > 16 eV [46]) and the broadband boron carbide focusing mirror (which has a high reflectivity for photon energies < 25 eV [47]). The XUV pulse energy at the source was approximately 350 nJ, as measured by an XUV photodiode (AXUV100G, Opto Diode). Taking into account the transmission through the Al filter (40%) and the reflectivity of the XUV focusing mirror (25%), an XUV pulse energy of 35 nJ is estimated on target. The XUV pulse duration is estimated as 25 fs, considering that the nonlinear HHG process typically leads to an XUV pulse duration which is approximately half the driving laser pulses duration, see e.g. [48, 49]. An XUV pulse duration of 25 fs was also obtained in HHG simulations when using 800 nm driving pulses [40].

To demonstrate the high intensity of our XUV source, we performed a nonlinear ionization experiment in Ar atoms. This target was chosen, because it allows a comparison with other experiments performed at FELs [1, 3] and using intense HHG sources [4, 6]. To this end, the XUV pulses were focused using a spherical mirror with a focal length of $f = 75$ mm. As shown in figures 4(a) and (b), both Ar²⁺ and Ar³⁺ ions were generated. The energy required to generate Ar²⁺ is 43.4 eV, and the energy required to generate Ar³⁺ is 84.1 eV [45], meaning that at least two and four XUV photons need to be absorbed to

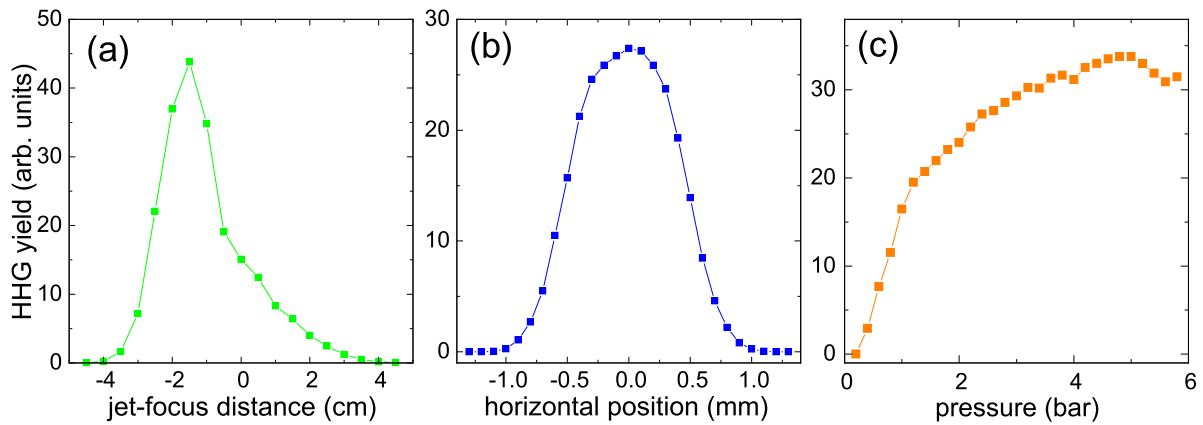


Figure 2. (a) HHG yield obtained in Kr using a backing pressure of 4 bar as a function of the distance between the gas jet and the focal plane of the driving laser. The maximum yield corresponds to about 10^{11} photons at the source. Negative distances correspond to the gas jet being placed behind the driving laser focus. The laser intensity of the violet beam at the focus when the gas jet is switched off is estimated as $8 \times 10^{15} \text{ W cm}^{-2}$ (b) HHG yield as a function of the transverse position of the gas jet at a jet-focus distance of -1.5 cm and a backing pressure of 4 bar. (c) HHG yield as a function of the backing pressure at a jet-focus distance of -1.5 cm .

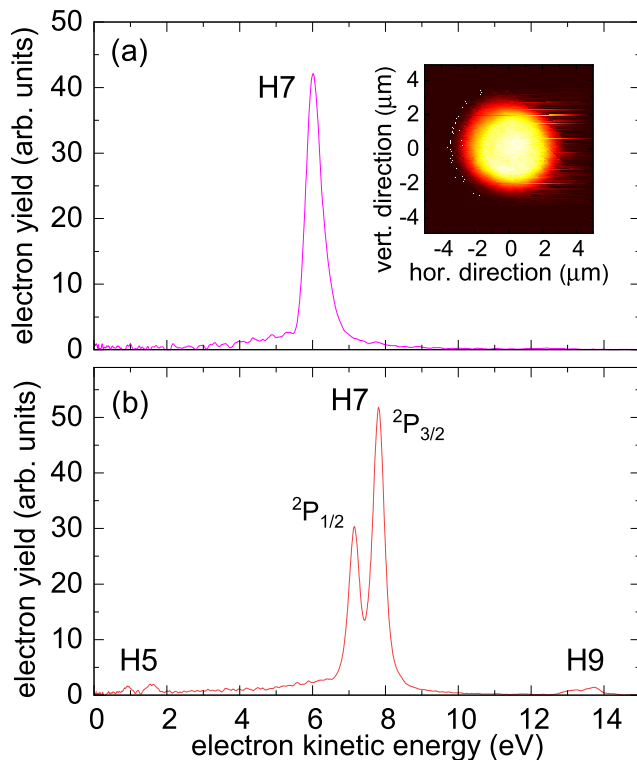


Figure 3. Photoelectron spectra measured for the ionization of (a) Ar and (b) Kr after focusing by the B_4C -coated spherical mirror. The spectra are dominated by contributions from the 7th harmonic (H7) at a photon energy of 22 eV. Spin-orbit splitting is visible in the photoelectron spectrum of Kr, where the two peaks correspond to the $^2P_{1/2}$ and $^2P_{3/2}$ states. The inset in (a) shows the XUV beam profile recorded 50 cm behind the gas jet.

generate Ar^{2+} and Ar^{3+} , respectively. We note that ionization may also take place via intermediate excited ionic states [45]. In figures 4(a) and (b), the spatial distributions of the different ion species are presented as a function of the distance from the XUV focal plane. These distributions are centered at the XUV focal plane, reflecting the nonlinear nature of the ionization

process. The narrower distribution of the Ar^{3+} ion trace compared to the Ar^{2+} ion trace is a consequence of the higher order of nonlinearity involved in the former case. The spatially resolved ion traces allow us to determine the relative ion yields at the XUV focal plane, giving an $\text{Ar}^{2+}/\text{Ar}^+$ ion yield ratio of 8% and an $\text{Ar}^{3+}/\text{Ar}^{2+}$ ion yield ratio of 17%.

The transversely integrated Ar^{2+} ion yield shown in figure 4(c) (red curve) is used to estimate the XUV Rayleigh length z_R . According to figure 4(d), where the Ar^{2+} yield is shown as a function of the XUV intensity, the generation of Ar^{2+} is a two-photon process. Therefore, the Ar^{2+} ion yield as a function of the distance z from the XUV focal plane is proportional to $(1 + z^2/z_R^2)^{-1}$ [40]. The measured ion distribution is further influenced by the spatial resolution of our method, see black curve in figure 4(c). The spatial resolution was estimated by the transverse width of the Ar^{2+} ion distribution at the XUV focal plane. After performing a deconvolution, the blue curve is obtained, which yields a Rayleigh length of $17 \mu\text{m}$. This allows us to estimate the XUV beam waist radius according to $w_0 = w_{\text{XUV,mirror}}(1 + d_{\text{XUV}}^2/z_R^2)^{-1/2} = (1.3 \pm 0.2) \mu\text{m}$, where $w_{\text{XUV,mirror}} = 6 \text{ mm}$ is the estimated XUV beam radius on the focusing mirror and $d_{\text{XUV}} = 81 \text{ mm}$ is the distance between the mirror and the imaging plane. We note that an imperfect alignment of the spherical mirror leading to astigmatism might affect the estimate of w_0 . Using $w_0 = 1.3 \mu\text{m}$, an XUV peak intensity of $5 \times 10^{13} \text{ W cm}^{-2}$ would be obtained. Our results are thus consistent with previous FEL results reported at a photon energy of 20 eV, where Ar^{3+} was the highest charge state at an intensity of $5 \times 10^{13} \text{ W cm}^{-2}$ [3]. In our previous experiment performed at an 18 m-long HHG beamline, Ar^{3+} ions were only observed at intensities of $1 \times 10^{14} \text{ W cm}^{-2}$ and higher [6]. The higher intensity required for the observation of Ar^{3+} in that experiment can be attributed to the much shorter XUV pulse duration of about 3 fs in that case [34], meaning that significantly less XUV photons are absorbed before the peak of the XUV intensity is reached. In contrast to the previously mentioned results, Ar^{3+} was only observed at XUV intensities exceeding $1 \times 10^{15} \text{ W cm}^{-2}$ using

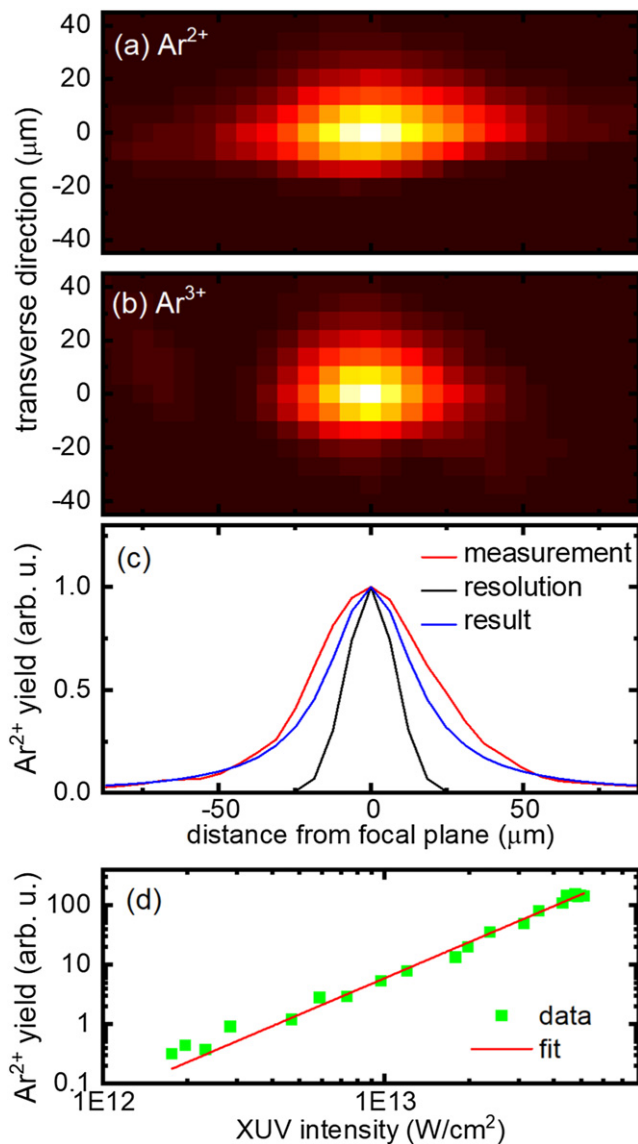


Figure 4. Distributions of (a) Ar^{2+} and (b) Ar^{3+} ions as a function of the distance from the XUV focal plane. The Ar^{3+} ion distribution is narrower because of the higher degree of nonlinearity involved. (c) Integrated Ar^{2+} ion yield (red curve), spatial resolution (black curve) and their deconvolution (blue curve). See text for details. (d) Ar^{2+} ion yield Y as a function of the XUV intensity (green squares) and a fit according to $Y \propto I^n$ (red curve), where I refers to the XUV peak intensity. A nonlinearity of $n = 2.0$ is obtained.

the intense XUV source based on HHG reported in reference [4]. This result was attributed to the higher degree of coherence of HHG sources compared to FEL sources, but is not corroborated by the results reported here.

In summary, we have reported on the generation of intense narrowband XUV pulses in a compact and simple setup, which is driven by 395 nm pulses with a moderate pulse energy of 3 mJ. Compared to our previous results, where four different harmonics were used for the nonlinear ionization of atoms [40], an important advantage of the current results are that the XUV pulse is dominated by a single harmonic. It is straightforward to implement this concept in many laboratories, since no large laboratories or multi-terawatt laser systems are needed,

in contrast to many state-of-the-art intense XUV sources based on HHG [4–6, 16, 30–32, 38]. Our results could therefore boost research fields that require intense XUV pulses such as XUV strong-field physics and CDI of nanoscale particles and nanostructures, thereby overcoming the challenges experienced in approaches where several harmonic orders are used [25]. In comparison to setups where a multilayer XUV mirror is used to select a single harmonic order [23], an advantage of the scheme presented here is the higher pulse energy that is contained in each harmonic order. By spectrally tuning either the fundamental laser or the second harmonic, tunable intense XUV pulses can be obtained and can be used to scan across resonances, similar to the way that this can be done at FELs [50]. Instead of the second harmonic, it is also possible to use the third harmonic for HHG [51, 52], allowing access to different harmonic orders and resulting in an even larger spacing between the individual harmonic orders.

ORCID iDs

M J J Vrakking  <https://orcid.org/0000-0002-3249-1663>

B Schütte  <https://orcid.org/0000-0001-5312-4611>

References

- [1] Wabnitz H, de Castro A R B, Gürtler P, Laarmann T, Laasch W, Schulz J and Möller T 2005 *Phys. Rev. Lett.* **94** 023001
- [2] Sorokin A A, Bobashev S V, Feigl T, Tiedtke K, Wabnitz H and Richter M 2007 *Phys. Rev. Lett.* **99** 213002
- [3] Motomura K *et al* 2009 *J. Phys. B: At. Mol. Opt. Phys.* **42** 221003
- [4] Nayak A *et al* 2018 *Phys. Rev. A* **98** 023426
- [5] Bergues B *et al* 2018 *Optica* **5** 237–42
- [6] Senftleben B *et al* 2020 *J. Phys.: Photonics* **2** 034001
- [7] Sorokin A A, Bobashev S V, Tiedtke K and Richter M 2006 *J. Phys. B: At. Mol. Opt. Phys.* **39** L299–304
- [8] Jiang Y H *et al* 2009 *Phys. Rev. Lett.* **102** 123002
- [9] Wabnitz H *et al* 2002 *Nature* **420** 482
- [10] Iwayama H *et al* 2010 *J. Phys. B: At. Mol. Opt. Phys.* **43** 161001
- [11] Schütte B, Arbeiter M, Fennel T, Vrakking M J J and Rouzée A 2014 *Phys. Rev. Lett.* **112** 073003
- [12] Helk T *et al* 2021 *Sci. Adv.* **7** eabe2265
- [13] Ott C *et al* 2019 *Phys. Rev. Lett.* **123** 163201
- [14] Ding T *et al* 2019 *Phys. Rev. Lett.* **123** 103001
- [15] Tzallas P, Skantzakis E, Nikolopoulos L A A, Tsakiris G D and Charalambidis D 2011 *Nat. Phys.* **7** 781
- [16] Takahashi E J, Lan P, Mücke O D, Nabekawa Y and Midorikawa K 2013 *Nat. Commun.* **4** 2691
- [17] Schnorr K *et al* 2014 *Phys. Rev. Lett.* **113** 073001
- [18] Meyer M *et al* 2010 *Phys. Rev. Lett.* **104** 213001
- [19] Varvarezos L *et al* 2021 *Phys. Rev. A* **103** 022832
- [20] Bencivenga F *et al* 2015 *Nature* **520** 205–8
- [21] Harries J R *et al* 2018 *Phys. Rev. Lett.* **121** 263201
- [22] Flögel M, Durá J, Schütte B, Ivanov M, Rouzée A and Vrakking M J J 2017 *Phys. Rev. A* **95** 021401
- [23] Ravasio A *et al* 2009 *Phys. Rev. Lett.* **103** 028104
- [24] Bostedt C *et al* 2012 *Phys. Rev. Lett.* **108** 093401
- [25] Rupp D *et al* 2017 *Nat. Commun.* **8** 493
- [26] Ackermann W *et al* 2007 *Nat. Photon.* **1** 336–42
- [27] Shintake T *et al* 2008 *Nat. Photon.* **2** 555–9
- [28] Allaria E *et al* 2012 *Nat. Photon.* **6** 699–704

- [29] Mashiko H, Suda A and Midorikawa K 2004 *Opt. Lett.* **29** 1927–9
- [30] Manschwetus B *et al* 2016 *Phys. Rev. A* **93** 061402
- [31] Hort O *et al* 2019 *Opt. Express* **27** 8871–83
- [32] Kühn S *et al* 2017 *J. Phys. B: At. Mol. Opt. Phys.* **50** 132002
- [33] Motoyama H, Iwasaki A, Takei Y, Kume T, Egawa S, Sato T, Yamanouchi K and Mimura H 2019 *Appl. Phys. Lett.* **114** 241102
- [34] Major B *et al* 2020 *J. Phys.: Photonics* **2** 034002
- [35] Kobayashi Y, Sekikawa T, Nabekawa Y and Watanabe S 1998 *Opt. Lett.* **23** 64–6
- [36] Sekikawa T, Kosuge A, Kanai T and Watanabe S 2004 *Nature* **432** 605–8
- [37] Barillot T R, Matia-Hernando P, Greening D, Walke D J, Witting T, Frasinski L J, Marangos J P and Tisch J W G 2017 *Chem. Phys. Lett.* **683** 38–42
- [38] Li J *et al* 2020 *J. Phys. B: At. Mol. Opt. Phys.* **53** 145602
- [39] Poletto L, Frassetto F, Calegari F, Anumula S, Trabattoni A and Nisoli M 2013 *Opt. Express* **21** 13040–51
- [40] Major B, Ghafur O, Kovács K, Varjú K, Tosa V, Vrakking M J J and Schütte B 2021 *Optica* **8** 960–5
- [41] Gademann G, Plé F, Paul P-M and Vrakking M J J 2011 *Opt. Express* **19** 24922
- [42] Irimia D, Dobrikov D, Kortekaas R, Voet H, van den Ende D A, Groen W A and Janssen M H M 2009 *Rev. Sci. Instrum.* **80** 113303
- [43] Eppink A T J B and Parker D H 1997 *Rev. Sci. Instrum.* **68** 3477
- [44] Stei M, von Vangerow J, Otto R, Kelkar A H, Carrascosa E, Best T and Wester R 2013 *J. Chem. Phys.* **138** 214201
- [45] Kramida A, Yu R and Reader J (NIST ASDTeam) 2021 *NIST Atomic Spectra Database (ver. 5.9)* (Gaithersburg, MD: National Institute of Standards and Technology) Available: <http://physics.nist.gov/asd> (19 November 2021)
- [46] Henke B L, Gullikson E M and Davis J C 1993 *At. Data Nucl. Data Tables* **54** 181–342
- [47] Larruquert J I and Keski-Kuha R A M 1999 *Appl. Opt.* **38** 1231–6
- [48] Mauritsson J *et al* 2004 *Phys. Rev. A* **70** 021801
- [49] Nabekawa Y, Hasegawa H, Takahashi E J and Midorikawa K 2005 *Phys. Rev. Lett.* **94** 043001
- [50] Takanashi T *et al* 2017 *Phys. Rev. Lett.* **118** 033202
- [51] Adachi S, Horio T and Suzuki T 2012 *Opt. Lett.* **37** 2118–20
- [52] Popmintchev D *et al* 2015 *Science* **350** 1225–231